Residual Stress Simulation of Injection Molding

Huamin Zhou, Guodong Xi, and Fen Liu

(Submitted August 14, 2006; in revised form June 16, 2007)

In this study, distribution and history of residual stresses in plaque-like geometries are simulated based on linear thermoviscoelastic model, which helps to understand the mechanics and evolution of the residual stresses in the injection molding process. The numerical calculation of direction, combined with the specified boundary conditions. Results show that the stress variation across the thickness exhibits a high surface tensile value changing to a compressive peak value close to the surface, with the core region experiencing a parabolic tensile peak. Residual stress distribution throughout the thickness is almost same along the flowpath and the final residual stresses value near the gate is lower than the value near the end of flowpath.

1. Introduction

Injection molding is a flexible production technique for the manufacturing of polymer product. A typical injection molding process consists of four stages: filling stage, packing stage, cooling stage, and ejection of the mold. During these processes, the residual stresses are produced due to high pressure and cooling, which induce the warpage and shrinkage. To yield the product with high precision, it is important to simulate the pressure- and thermal-induced residual stresses in the processes.

Residual stresses of injection molding have received more and more attention recently. Many researchers calculated the residual stresses and shrinkage by using different models. For example, Bushko and Stokes (Ref 1, 2) investigated the problem of solidification of a molten polymeric material between cooled parallel plates to study the mechanics of part shrinkage and warpage and the buildup of residual stresses in the injection molding process. An orthotropic thermo-rheologically simple viscoelastic model was assumed. Packing pressure effect was assessed by introducing the reference strain. Jansen and Titomanlio (Ref 3, 4) calculated residual stresses using a simple elastic model. The pressure effect has been included in the analysis. In this model, all relaxation effects are neglected. Thus the model overestimated calculated stress. Kamal et al. (Ref 5) analyzed the thermal stress in the thin wall moldings using the models that assume linear thermoelastic and linear thermoviscoelastic behavior of polymeric materials. Polymer crystallization effects on stresses are examined. Zoetelief and Douven (Ref 6) simulated the thermal residual stress using a linear viscoelastic constitutive model in the holding stage and compared the results with the experimental results.

In general, existing studies on the residual stresses focused on the theory analysis and isolated model, without combining with the characteristic of the injection molding and integrating with the packing and cooling analysis. In this study, distribution and history of residual stresses in plaque-like geometry are simulated by using the same material model as that of Zoetelief (Ref 6). In the simulation, both the packing and cooling stages are considered so that effects of pressure and thermal history and stress relaxation are taken into account. The numerical calculation model is built by finite difference method in the time and layer discretization in the thickness direction, combined with the proposed specified boundary conditions. The developed simulation system is used to calculate the residual stresses of the typical injection parts. To verify the modeling, calculation results are compared with the experiment results in Ref 6.

2. Modeling and Implementation

2.1 Linear Thermoviscoelastic Model

Thermally and pressure-induced stresses arise from inhomogeneous cooling of the part in combination with the hydrostatic pressure. On cooling, the relaxation time increases and becomes comparable to the process time. Therefore accurate predictions of thermal stresses would require viscoelastic constitutive equations. In the limit of infinitesimal strains, the behavior of viscoelastic materials is well described by the theory of linear viscoelasticity. Because the most injection molding products are very thin, we can take the flow direction as the 1-direction and the local thickness direction as the 3-direction and build the local coordinates. The total stress tensor can be split into a hydrostatic pressure and an extra stress part (Ref 6, 7):

$$\sigma_{ij} = -P_h I + \tau_{ij} \tag{Eq 1}$$

$$P_h = -\frac{1}{3} T_r \sigma = -\int_{-\infty}^{t} G_1(\varsigma(t) - \varsigma(t')) \left(\frac{\partial \varepsilon_m}{\partial t'} - \frac{\partial \varepsilon_{th}}{\partial t'} \right) dt' \tag{Eq 2}$$

Huamin Zhou, Guodong Xi, and **Fen Liu**, State Key Lab. of Mold & Die Technology, Huazhong University of Science and Technology, Wuhan, Hubei 430074, People's Republic of China. Contact e-mail: hmzhou@263.net.

$$\tau_{ij}(t) = \int_{-\infty}^{t} G_2(\varsigma(t) - \varsigma(t')) \frac{\partial \varepsilon_{ij}^{d}}{\partial t'} dt' \qquad \text{(Eq 3)}$$

where P_h is the hydrostatic pressure and equals to negative spherical tensor, τ_{ij} is the extra stress tensor, G_1 is bulk relaxation function, G_2 is shear relaxation function, ε_{th} is thermal strain, ε_m is spherical stain tensor, ε_{ij}^{d} is extra stain tensor and $\varsigma(t)$ is material time.

To briefly comment on the relaxation functions G_1 and G_2, let $3K$ and $2G$ denote the value of G_1 and G_2 at time $t = 0$, respectively (Ref 8):

$$G_1(t) = \frac{E}{1 - 2u} \varphi(t) = 3K\varphi(t) \qquad \text{(Eq 4)}$$

$$G_2(t) = \frac{E}{1 + u} \varphi(t) = 2G\varphi(t) \qquad \text{(Eq 5)}$$

where E and μ are Young's modulus and Poisson's ratio, respectively. K and G are bulk and shear modulus, respectively. Both G_1 and G_2 depend on the same relaxation function $\varphi(t)$. The relaxation function is approximated as a sum of weighted exponential functions:

$$\varphi(t) = \sum_{k=1}^{N} g_k \exp\left(-\frac{t}{\lambda_k}\right) \qquad \text{(Eq 6)}$$

where λ_k and g_k are the relaxation spectrum and in which $\sum_{k=1}^{N} g_k = 1$.

It is assumed that initial stain and stress are undisturbed for all when $t < 0$. By applying Eq 4 to Eq 2, the hydrostatic pressure can be expressed as

$$P_h = \int_{0}^{t} 3K\varphi(\varsigma(t) - \varsigma(t'))\left(\frac{\partial \varepsilon_{th}}{\partial t'} - \frac{\partial \varepsilon_m}{\partial t'}\right) dt'$$
$$= \int_{0}^{t} 3K\varphi(\varsigma(t) - \varsigma(t'))\frac{\partial \varepsilon_{th}}{\partial t'} dt' - \int_{0}^{t} K\varphi(\varsigma(t) - \varsigma(t'))\frac{3\partial \varepsilon_m}{\partial t'} dt' \qquad \text{(Eq 7)}$$

Thermal strain is given by:

$$\varepsilon_{th} = \int_{0}^{t} \alpha(\bar{t}) \frac{\partial T(\bar{t})}{\bar{t}} d\bar{t} \qquad \text{(Eq 8)}$$

where α is thermal expansion coefficient. If α is constant, the thermal strain can be written as

$$\varepsilon_{th} = \alpha \int_{0}^{t} \frac{\partial T(\bar{t})}{\bar{t}} d\bar{t} \qquad \text{(Eq 9)}$$

Substituting Eq 5 into Eq 3 results in:

$$\tau_{ij}(t) = 2 \int_{-\infty}^{t} G\varphi(\varsigma(t) - \varsigma(t')) \frac{\partial \varepsilon_{ij}^{d}}{\partial t'} dt' \qquad \text{(Eq 10)}$$

where extra strain tensor is given by:

$$\varepsilon_{ij}^{d} = \varepsilon_{ij} - \frac{1}{3} T_r \varepsilon \delta_{ij} \qquad \text{(Eq 11)}$$

To wish to briefly comment, let $K(t) = K\varphi(t)$, $\beta(t) = 3\alpha K\varphi(t)$, and $G(t) = G\varphi(t)$.

Substituting $T_r\varepsilon = \varepsilon_{11} + \varepsilon_{22} + \varepsilon_{33} = 3\varepsilon_m$ into Eq 7 results in:

$$P_h = \int_{0}^{t} \left(\beta(\varsigma(t) - \varsigma(t'))\frac{\partial T}{\partial t'} - K(\varsigma(t) - \varsigma(t'))\frac{\partial T_r \varepsilon_m}{\partial t'}\right) dt' \qquad \text{(Eq 12)}$$

$$\tau_{ij} = 2 \int_{0}^{t} G(\varsigma(t) - \varsigma(t')) \frac{\partial \varepsilon_{ij}^{d}}{\partial t'} dt' \qquad \text{(Eq 13)}$$

In Eq 2, 3, 12, and 13, $\varsigma(t)$ is material time and defined as

$$\varsigma(t) = \int_{0}^{t} \frac{1}{\alpha_T} dt' \qquad \text{(Eq 14)}$$

where α_T is the time-temperature shift factor. For amorphous materials with temperatures raging from glass transition temperature to 100 °C above glass transition temperature, the classic WLF (Ref 7) equation is used to describe the time-temperature shift factor:

$$\log_{10} \alpha_T = -\frac{c_1(T - T_r)}{c_2 + (T - T_r)} \qquad \text{(Eq 15)}$$

For temperatures outside the above range or for semicrystalline materials, an Arrhenius expression is chosen:

$$\ln \alpha_T = -c_3(T - T_r) \qquad \text{(Eq 16)}$$

where c_1, c_2, and c_3 are constants and T_r is a reference temperature.

2.2 Assumptions and Boundary Conditions

For simplifying the calculation of thermally and pressure-induced stresses in the injection molding process, the following assumptions are made:

(1) While in the mold, the materials are locally constrained in the in-plane directions by three dimensional features of the part (bosses, ribs, and other walls). The material is assumed to be constrained in the in-plane directions, so that in-plane strain $\varepsilon_{11} = \varepsilon_{22} = 0$.
(2) The normal stress σ_{33} is constant in the thickness direction.
(3) As long as the cavity pressure is nonzero ($\sigma_{33} < 0$), the materials stick to the mold walls.
(4) Mold elasticity is neglected.
(5) The warpage in the mold is not taken into account.

In injection molding process, the flow-induced stresses during the filling stage are an order of magnitude smaller than the thermally induced stresses (Ref 9). Therefore, flow-induced stress is neglected in a crude approximate model. In this study, only the packing and cooling stages of injection molding were considered for the analysis of residual stresses. It is assumed that the material is undisturbed for all $t < 0$. In the molding process, the local boundary conditions keep changing with time, including temperature, cavity pressure, and mold constraint. Zhou and Li (Ref 10) and Cui et al. (Ref 11) successfully simulated the temperature and pressure field of the packing stage and cooling stage using the surface mesh model, which provide the essential input for the presented residual stresses analysis. Differing from the four situations used as boundary conditions in Ref 6, the following different cases are considered for the local boundary conditions in terms of the normal stress σ_{33}:

(1) When packing stage begins, the molten material solidifies at the mold surface and there is coexistence of two solid skins and a liquid core, like sandwich. The normal stress equals the opposite of the cavity pressure. In this stage, the pressure can be controlled and be obtained by the packing simulation:

$$\sigma_{33} = -P \qquad \text{(Eq 17)}$$

(2) After packing stage or the gate completely froze, no more packing pressure is applied to the part to compensate for the volumetric shrinkage by cooling. In this case, cavity pressure still exists. Therefore, the material sticks to the mold walls and there is no change in thickness direction:

$$\int_{-l/2}^{l/2} \Delta\varepsilon_{33}(z)\mathrm{d}z = 0 \qquad \text{(Eq 18)}$$

(3) When cavity pressure drops to zero, material detaches from the walls and shrinks in the thickness direction until demolding.

2.3 Numerical Formulation

For the numerical solution of the residual stress problem, the linear thermoviscoelastic equation is written in a temporally discrete form. In this way, the stress state at time t_{n+1} can be evaluated from the known stress state at time t_n. First, Eq 12 can be written as

$$P_{\mathrm{h}}(t_{n+1}) = P_{\mathrm{h}}(t_n) + \beta\Delta T - KT_{\mathrm{r}}\Delta\varepsilon \qquad \text{(Eq 19)}$$

where ΔT and $\Delta\varepsilon$ are the change in temperature and strain respectively, during time step $\Delta t = t_{n+1} - t_n$.

Extra stress can be decomposed as

$$\tau_{11}(t) = \sum_{k=1}^{N} p_{11}^{(k)}(t) \qquad \text{(Eq 20a)}$$

$$\tau_{22}(t) = \sum_{k=1}^{N} p_{22}^{(k)}(t) \qquad \text{(Eq 20b)}$$

$$\tau_{33}(t) = \sum_{k=1}^{N} p_{33}^{(k)}(t) \qquad \text{(Eq 20c)}$$

where

$$p_{11}^{(k)}(t) = 2Gg_k \int_0^t \exp\left(-\frac{\varsigma(t) - \varsigma(t')}{\lambda}\right)\mathrm{d}\varepsilon_{11}^{\mathrm{d}}(t') \qquad \text{(Eq 21)}$$

Differentiate Eq 21 with respect to t, thus:

$$\frac{\mathrm{d}p_{11}}{\mathrm{d}t} + \frac{1}{\lambda}\frac{\mathrm{d}\varsigma}{\mathrm{d}t}p_{11} = 2Gg_k\frac{\mathrm{d}\varepsilon_{11}^{\mathrm{d}}}{\mathrm{d}t} \qquad \text{(Eq 22)}$$

The differential equation can then be discretized using a finite difference scheme which gives:

$$\frac{p_{11}(t_{n+1}) - p_{11}(t_n)}{\Delta t} + \frac{1}{\lambda}\frac{\Delta\varsigma}{\Delta t}p_{11}(t_{n+1}) = 2Gg_k\frac{\Delta\varepsilon_{11}^{\mathrm{d}}}{\Delta t} \qquad \text{(Eq 23)}$$

Equation 23 further can be expressed as

$$p_{11}^{(k)}(t_{n+1}) = \varsigma_k[p_{11}^{(k)}(t_n) + 2Gg_k\Delta\varepsilon_{11}^{\mathrm{d}}] \qquad \text{(Eq 24)}$$

where

$$\varsigma_k = \left(1 + \frac{\Delta\varsigma}{\lambda_k}\right)^{-1} \qquad \text{(Eq 25)}$$

Similar equations can be obtained:

$$p_{22}^{(k)}(t_{n+1}) = \varsigma_k[p_{22}^{(k)}(t_n) + 2Gg_k\Delta\varepsilon_{22}^{\mathrm{d}}] \qquad \text{(Eq 26)}$$

$$p_{33}^{(k)}(t_{n+1}) = \varsigma_k[p_{33}^{(k)}(t_n) + 2Gg_k\Delta\varepsilon_{33}^{\mathrm{d}}] \qquad \text{(Eq 27)}$$

Considering the incremental strain, basic assumption (1) $\Delta\varepsilon_{11} = \Delta\varepsilon_{22} = 0$ implies:

$$T_{\mathrm{r}}(\Delta\varepsilon) = \Delta\varepsilon_{11} + \Delta\varepsilon_{22} + \Delta\varepsilon_{33} = \Delta\varepsilon_{33} \qquad \text{(Eq 28)}$$

$$\Delta\varepsilon_{\mathrm{m}} = \frac{1}{3}(\Delta\varepsilon_{11} + \Delta\varepsilon_{22} + \Delta\varepsilon_{33}) = \frac{1}{3}\Delta\varepsilon_{33} \qquad \text{(Eq 29)}$$

$$\Delta\varepsilon_{11}^{\mathrm{d}} = \Delta\varepsilon_{11} - \Delta\varepsilon_{\mathrm{m}} = -\frac{1}{3}\Delta\varepsilon_{33} \qquad \text{(Eq 30)}$$

$$\Delta\varepsilon_{22}^{\mathrm{d}} = \Delta\varepsilon_{22} - \Delta\varepsilon_{\mathrm{m}} = -\frac{1}{3}\Delta\varepsilon_{33} \qquad \text{(Eq 31)}$$

$$\Delta\varepsilon_{33}^{\mathrm{d}} = \Delta\varepsilon_{22} - \Delta\varepsilon_{\mathrm{m}} = \frac{2}{3}\Delta\varepsilon_{33} \qquad \text{(Eq 32)}$$

Thus the normal stress component can be expressed as:

$$\sigma_{33}(t_{n+1}) = \sigma_{33}^* + \left(\frac{4}{3}G\sum_{k=1}^{N}\varsigma_k g_k + K\right)\Delta\varepsilon_{33} \qquad \text{(Eq 33)}$$

where σ_{33}^* is given by:

$$\sigma_{33}^* = -(P_{\mathrm{h}}(t_n) + \beta\Delta T) + \sum_{k=1}^{N}\varsigma_k p_{33}^{(k)}(t_n) \qquad \text{(Eq 34)}$$

Thus the incremental strain component $\Delta\varepsilon_{33}$ at the time interval can be calculated on the basis of Eq 33:

$$\Delta\varepsilon_{33} = \frac{\sigma_{33}(t_{n+1}) - \sigma_{33}^*}{\frac{4}{3}G\sum_{k=1}^{N}\varsigma_k g_k + K} \qquad \text{(Eq 35)}$$

According to above temporally discrete form, the stress state at time t_{n+1} can be evaluated from the known stress state at time t_n and boundary conditions. The calculation is performed element by element at each layer, based on the finite element mesh used in packing and cooling analysis and layers in the thickness direction. The computation procedure is summarized as follows:

(1) Based on the simulated temperature field result, calculate $\Delta T = T(t_{n+1}) - T(t_n)$ at t_{n+1};
(2) Calculate the time-temperature shift factor α_{T}, the material time step $\Delta\varsigma$ and $\varsigma_k (k = 1, 2, ..., N)$ based on Eq 15 and 16, Eq 14 and 25, respectively;
(3) Calculate the σ_{33}^*, substitute current hydrostatic pressure $P_{\mathrm{h}}(t_n)$ and step temperature change ΔT into Eq 34;
(4) Determine the normal stress component σ_{33} by the boundary conditions of different injection stage:

Case 1: If there is coexistence of solid layers and liquid core, the normal stress equals the opposite of the cavity pressure, σ_{33} can be obtained based on Eq 17:

$$\sigma_{33}(t_{n+1}) = -P(t_{n+1}) \qquad \text{(Eq 36)}$$

Case 2: When the material has solidified throughout the thickness, the material still sticks to the mold walls and the change in thickness direction is zero based on Eq 18 then:

$$\Delta l_0 = \sum_{i=1}^{N} \Delta\varepsilon_{33} l_0^{(i)} = 0 \qquad \text{(Eq 37)}$$

where $l_0^{(i)}$ is the initial thickness of layer i, substituting Eq 35 into Eq 37 results in:

$$\sigma_{33}(t_{n+1}) = \frac{\sum_{i=1}^{N} \frac{\sigma_{33}^*}{V} l_0^{(i)}}{\sum_{i=1}^{N} \frac{1}{V} l_0^{(i)}} \qquad \text{(Eq 38)}$$

where $V = \frac{4}{3} G \sum_{k=1}^{N} \varsigma_k g_k + K$.

Case 3: Cavity pressure drop to zero and the material detaches from the walls, so:

$$\sigma_{33}(t_{n+1}) = 0 \qquad \text{(Eq 39)}$$

(5) Calculate $\Delta\varepsilon_{33}$ by substituting current normal stress σ_{33} into Eq 35;
(6) Calculate extra strain tensor based on Eq 30, 31, and 32, and calculate hydrostatics pressure $P_h(t_{n+1})$ using Eq 19;
(7) Calculate extra stress tensor τ_{11}, τ_{22}, and τ_{33} based on Eq 20;
(8) Calculate σ_{11} and σ_{22} based on Eq 1.

3. Results and Verification

To study the evolution and distribution of the stresses, simulation is performed for a fan-gated specimen ($300 \times 75 \times 2.5$ mm^3), as shown in Fig. 1. A minimum complexity approach is proposed in this article to emphasize the process physics, which would result in a better understanding of the transition that takes place during the molding. The material used was ABS (Novodur P2X of Bayer). The material parameters and the main processing parameters are listed in Tables 1 and 2, respectively. Relaxation spectrum λ_k and g_k in Eq 6 are listed in Table 3. The material parameters used in time-temperature shift equations Eq 15 and 16 are listed in Table 4. All above material data were from Ref 6.

According to the basic assumptions (3) normal stress equals the negative of the packing pressure in the simulation. Therefore, the evolution of the cavity pressure shows the variety of the normal stress. Figure 2 shows the calculated pressure history at different locations along the flowpath, including the pressure profiles near the gate, quarter to the gate, halfway down to the end, quarter to the end, and near the end of the flowpath.

3.1 Evolution of Residual Stresses

To the transversely isotropic material, x-direction stress equals y-direction stress. Figures 3 and 4 show the in-plane stresses (stresses in the flow plane) distribution in the gapwise (thickness) direction and its evolution of the central position P1
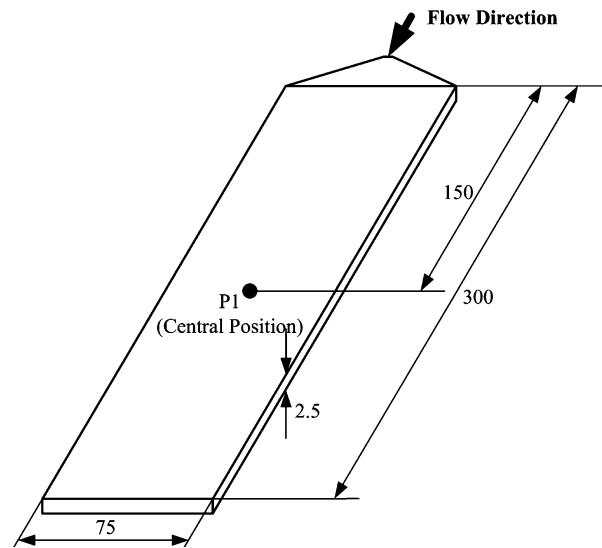

Fig. 1 Rectangular strip mold cavity (mm)

Table 1 Material properties

Material parameter	Value
Material brand	Novodur P2X
Producer	Bayer
Solidification temperature (K)	368
Thermal expansion coefficient (1/K)	8×10^{-5}
Young's modulus (MPa)	2240
Shear modulus (MPa)	805
Poisson's ratio	0.392

Table 2 Processing conditions of injection molding

Processing parameter	Value
Injection time (s)	1.2
Packing time (s)	6.3
Cooling time (s)	21.7
Melt temperature (K)	513
Mold temperature (K)	325
Packing pressure (MPa)	60

(marked in Fig. 1). Figure 3 shows the whole evolution of in-plane stresses. Figure 4 shows stresses distribution at five typical instants: (1) at the beginning of the filling stage; (2) at the end of the filling stage; (3) at the end of the packing stage; (4) when the pressure of the central position drops to zero; (5) just before ejection.

During filling, the melt material is forced into the mold. When the melt contacts the cold mold surface, a very thin layer solidifies quickly at the mold surface, in which the stress is induced as a result of material cooling. Below the surface, the stress distribution has a sharp decline. As shown in Fig. 4, the stress remains uniform over a central region in which the material is essentially in a rubbery state with low elastic modulus and equals the negative of the packing pressure. As the packing stage starts, in-plane stress continues to decrease and quickly reaches the lowest value as the quick increase of the cavity pressure. During packing, packing pressure forces

Table 3 Relaxation spectrum data

	1	2	3	4	5	6
λ_k (s)	4.706×10^{-9}	4.410×10^{-6}	2.082×10^{-3}	6.198×10^{-1}	3.035×10^{6}	2.749×10^{8}
g_k	5.014×10^{-2}	8.585×10^{-2}	2.869×10^{-1}	4.043×10^{-1}	3.531×10^{-4}	1.171×10^{-4}

Table 4 Parameters in time-temperature shift functions

Parameter	Value
c_1	14.22
c_2 (K)	47.01
c_3 (K^{-1})	0.3291
T_r (K)	373
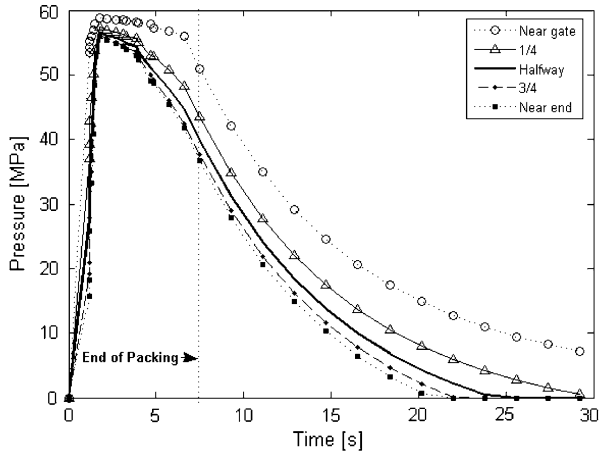
Fig. 2 Calculated pressure history at different locations along the flowpath
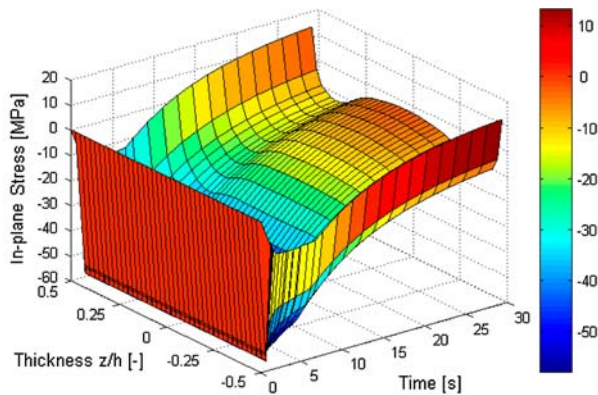
Fig. 3 In-plane stress distribution and evolution of Point P1

Fig. 4 In-plane stress distribution in the gapwise direction at five typical instants of Point P1

Fig. 5 In-plane stress distribution in the gapwise direction along the flowpath after ejection

the melt material into the mold to compensate for the volumetric shrinkage that occurs during cooling. In-plane stress in the core region mainly holds constant at first, and then slowly decays as the cavity pressure. Moreover, the stress evolution corresponds to the evolution of the cavity pressure in Fig. 2. The stress in the constrained solidified layers increases as a result of temperature decreases. At the end of the packing, the shape of the distribution changes and shows that relative high stresses have been built up in the surface layer, followed by a
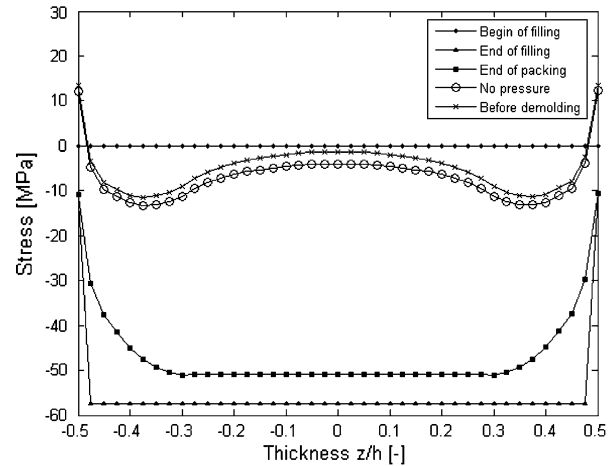
sharp decline in the region more inward. Stresses in central region still remain uniform. Then, no more packing pressure is applied to the part and the cavity pressure drop quickly, which causes the compressive stress begins to decrease throughout the product. Just before ejection, the residual stress distribution consists of three distinct regions made up of two skins and a core. The stress exhibits a high surface tensile value and changes to a compressive peak value close to the surface, with the core region experiencing a parabolic peak.

3.2 In-plane Residual Stresses Distribution in Flowpath

In the injection molding, the pressure history and temperature history at different location are not same, which causes an un-uniform distribution of the in-plane stress. Figure 5 shows the predicted final in-plane stresses distributions in the gapwise direction along the flowpath after ejection. The shapes of the
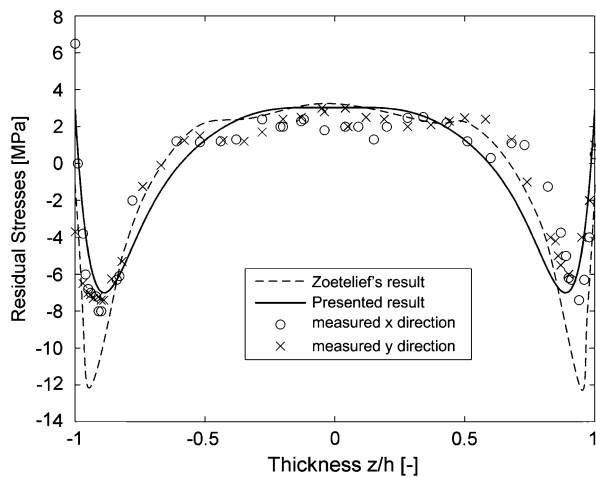
Fig. 6 Calculated and measured in-plane stress distribution in the gapwise direction

stresses distribution in the gapwise direction are almost the same along the flowpath. However, the central tensile stresses near the gate are littler lower than the stresses at the locations away from the gate.

3.3 Experimental Verification

Measurements of residual stresses are frequently carried out with the layer removal method. This method is relatively easy to apply to flat specimens and gives information about the stress distribution in the gapwise direction. Zoetelief (Ref 6) successfully applied this method to the specimens and the experimental data are used for verification in this article.

As shown in Fig. 6, the calculated stresses profiles are compared with Zoetelief's experimental values and simulation results (Ref 6). In the calculation, material and processing parameters are same to the Zoetelief's experiment. There is a qualitative agreement between the measured and the calculated results. Moreover, to the amorphous polymer, the calculated in-plane stresses in *x* and *y* directions are the same, since anisotropy is not taken into account. It can be seen that there is a peak at the subsurface region in the simulation results of Zoetelief, which has been improved observably in this article with more reasonable treatment of the boundary conditions.

4. Conclusion

In the present study, the evolution and the distribution along the flowpath of the cavity pressure and residual stresses are simulated. Calculations with a viscoelastic mode are compared with experimental results obtained with the layer removal method for ABS specimens. Calculations show

in-plane stresses distribution in the thickness direction varies greatly in the injection molding process.

At the beginning, there are considerable higher stresses in the skin region, while stresses drop quickly below the surface and remain uniform over a central region. Just before ejection, the stresses exhibit a high surface tensile value and change to a compressive peak value close to the surface, with the core region experiencing a parabolic tensile peak. During the process, the shapes of the stresses distribution in the gapwise direction are almost the same along the flowpath. At the beginning, there is a significant difference of the stresses value along the flowpath and then stresses tend to be uniform. After ejection, the central tensile stresses near the gate are little lower than the stresses at the locations away from the gate.

References

1. W.C. Bushko and V.K. Stokes, Solidification of Thermoviscoelastic Melts. Part I. Formulation of Model Problem, *Polym. Eng. Sci.*, 1995, **35**(4), p 351–364
2. W.C. Bushko and V.K. Stokes, Solidification of Thermoviscoelastic Melts. Part II: Effects of Processing Conditions on Shrinkage and Residual Stresses, *Polym. Eng. Sci.*, 1995, **35**(4), p 365–383
3. K.M.B. Jansen and G. Titomanlio, Effect of Pressure History on Shrinkage and Residual Stresses-Injection Molding with Constrained Shrinkage, *Polym. Eng. Sci.*, 1996, **36**(15), p 2029–2040
4. G. Titomanlio and K.M.B. Jansen, In-Mold Shrinkage and Stress Prediction in Injection Molding, *Polym. Eng. Sci.*, 1996, **36**(15), p 2041–2049
5. M.R. Kamal, R.A. Lai-Fook, and J.R. Hernandez-Aguilar, Residual Thermal Stresses in Injection Moldings of Thermoplastics: A Theoretical and Experimental Study, *Polym. Eng. Sci.*, 2002, **42**(5), p 1098–1114
6. W.F. Zoetelief and L.F.A. Douven, Residual Thermal Stresses in Injection Molded Products, *Polym. Eng. Sci.*, 1996, **36**(14), p 1886–1896
7. J.D. Ferry, *Viscoelastic Properties of Polymers*. 3rd ed., Wiley, New York, 1980
8. K.K. Kabanemi, H. Vaillancourt, H. Wang, and G. Salloum, Residual Stresses, Shrinkage, and Warpage of Complex Injection Molded Products: Numerical Simulation and Experimental Validation, *Polym. Eng. Sci.*, 1998, **38**(1), p 21–37
9. X. Chen, Y.C. Lam, and D.Q. Li, Analysis of Thermal Residual Stress in Plastic Injection Molding, *J. Mater. Process. Technol.*, 2000, **101**(1), p 275–280
10. H.M. Zhou and D.Q. Li, A Numerical Simulation of the Filling Stage in Injection Molding Based on a Surface Model, *Adv. Polym. Technol.*, 2001, **20**(2), p 125–131
11. S.B. Cui, H.M. Zhou, and D.Q. Li, Numerical Simulation of Injection Molding Cooling Process Based on 3D Surface Model, *Comput. Aided Drafting Design Manuf.*, 2004, **14**(2), p 64–70